

Selection mutation rates are the maximal robustness rates of non-stationary environments

Andre F. Ribeiro¹ (ribeiro@alum.mit.edu)

¹University of Sao Paulo, Sao Carlos, SP, 13560-970, Brazil

Distinct population structures offer their populations adaptations with distinct robustness (i.e., effect generalizability across members). We demonstrate that populations under (1) drift and (2) selection have mutation rates and population structures that correspond to the maximal-generalization rates and structures of, respectively, (1) stationary (constant) and (2) non-stationary (changing) environments. We employ both broad time, large-scale genome sequencing datasets (including whole-genome autocorrelation calculations at unprecedented scales), and fine time-scale barcoding experiments.

1 Introduction

Increasing evidence points to the shaping influence of mutation robustness (i.e., the external validity of mutation effects across population members) on the adaptation process¹⁻⁸. Theoretically, the relationship between the evolutionary process and robustness⁹⁻¹⁴, or, the process and arbitrary population-structures¹⁵⁻¹⁷ have remained highly idealized, often accompanied of only simulated or, more commonly, no evidence. Robustness is typically quantified in a simple way^{18,19} (e.g., the number of members with overlapping phenotypes in a population), but is related to quickly developing issues of generalization in Machine Learning and Statistics. Here, we review the theory behind robustness, its relation to adaptation under pleiotropy, and reconsider recent and popular data in light of the resulting model.

We can introduce the problem using Fisher's famous allegory for multi-dimensional adaptation with pleiotropy²⁰⁻²². A microscope's performance at an instant is a function of its various knobs' positions, like an organism of its traits (e.g., body size, beak length). The process of random, and time-extended, adaptation is then analogous to one where we randomly change knob positions, until a sharp image comes through, Fig.1(a). Fitness gains and losses brought by any mutation are, however, contingent on a large number of factors (environmental, developmental, regulatory, etc.) Each fitness observation is thus valid only in its very instantaneous set of conditions. Since gains from a knob depends on the position of all other knobs, the only sure-way to assure no false-positive adaptations is to try each knob position, in each variation of all other knobs. This is illustrated by the wheel in Fig.1(b), which generates all possible knob variations by phasing their rotations. We call this alternative to Fisher's Geometrical Model (FGM) the Latin-Square Model (LSM).

The FGM is a full randomization approach, where we randomly switch knobs, and approach

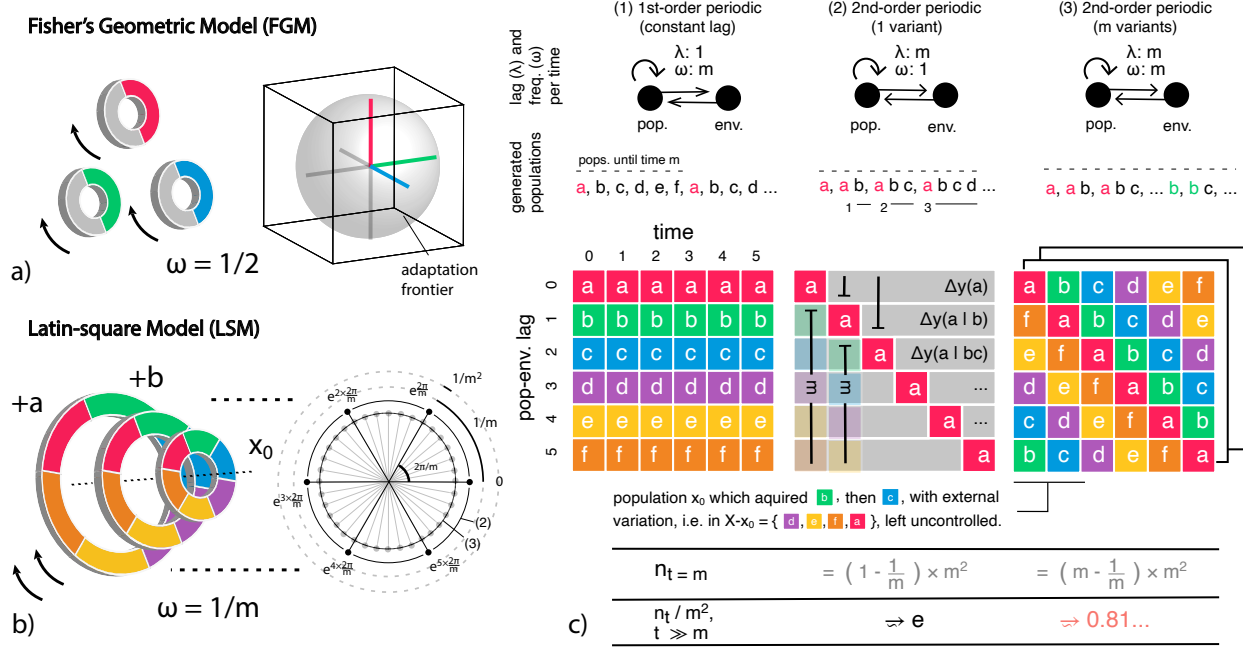


Figure 1 Latin Square Model (LSM). (a) Fisher's Geometric Model (FGM) and microscope analogy, (b) LSM as a mechanism to generalize mutation effects across populations, and (right) its whole genome frequency-based representation, (c) population-environment systems (1-3) with $m = 6$ environmental changes (colored Latin-letters) and distinct per-time lags and frequencies, their associated (middle) Latin-Squares, and, (lower table) per-variant mutation rates.

the instrument non-methodically. The LSM is closer to how a microscope is actually used, where we change a given knob, while systematically fixing all other knobs' values, in a 'structured randomization' approach that is akin to simultaneous experimentation. While the FGM makes many assumptions (strong stabilizing selection, haploid populations, equal effect mutations, etc.) the one that washes away issues of robustness is that there are no mutational correlations among traits^{20,22}. In more realistic conditions, moving a knob would move many other knobs, in unknown ways. The microscope's design, like the experimental, is an apt abstraction because it breaks down all possible variations available to its operator in dimensions whose effects remain unconfounded throughout adaptation. Exactly because of this assumption of independence, Fisher was able to model adaptation as trajectories in Euclidean m -dimensional spaces, finally showing that adaptation largely takes place in a sphere around the optimal, Fig.1(a). In both models, FGM and LSM, mutation effects are commutable. In Fisher's model this requires a statistical independence assumption, while, in the LSM, commutation is afforded by population structure - taken as part of the adaptation process itself. Such questions are fundamental, as they cut to the core of what selection and adaptation are about: populations' ability to quickly identify the effects of previously unseen, or 'untested', mutations.

The LSM, further introduced below, has five key advantages, which make it uniquely suited to empirical research,

- **Non-parametric.** The LSM is a direct implication, and not a theoretical model, of the population-environment combinatorial structure. It requires and makes no complex parametric assumptions.
- **Effects from the ground-up.** Theoretical models often have hypotheticals (fitness landscapes, phenotypic multi-dimensional spaces, effective populations, phenotype-genotype graphs, etc.) that make them difficult to validate. The LSM is formulated entirely from (correlated, confounded, etc.) observed effects of mutations on phenotypes, which are readily observed in experimental datasets, and estimated in observational.
- **Full-genome scale.** Models of adaptation often consider mutations at a single site, gene or small genome. Mutation rates are, however, a population characteristic, and periodic or multi-scale patterns, like the ones below, are biased, phased, or disappear in genomic segments. Using large-scale computation, we consider combinatorial patterns across the many whole-genomes in populations.
- **Representational role of single genomes.** As the sole source of genomic changes, mutations have a key role in explaining how populations use genomes to collectively represent (and react to) their environments. This vital population-environment connection has been increasingly de-emphasized with the availability of packaged omnic data, but is formulated explicitly in the LSM.

- **Theoretically consistent.** The LSM is consistent with mainstream models; being, in fact, a statistical re-interpretation of Moran and Wright-Fisher models (and the FGM)²³, while adding to these models sophisticated statistical tools to articulate and quantify populations' mutation robustness.

Population rate-of-change under external change. Consider a population in an environment that is changing at a rate of ω_{env} . A critical question is how that population should choose its own rate of change ω_{pop} , in response. Together, the population and environment make up a reciprocal system, where the environment has m variations - labeled $X = \{a, b, c, \dots, [m]\}$ - that can affect the population's fitness $y \in \mathbb{R}$. Consider then how alternative ω_{pop} rates affects populations' ability to adapt, in particular, in respect to the number and types of effects they observe as result. Fig.1(c) depicts three cases: (1) fixed population-environment lag, (2) m periodic lag (per variant), and, (3) m frequency. The in-phase case, (1), is depicted by the lag vs. time matrix in Fig.1(c, left). Effects for a are observed there in only one background condition*, $\Delta y(a \mid b = 0, c = 0, d = 0, \dots)$, repeatedly (across all times and populations). Any changes in factors (b, c, d, \dots), will likely invalidate these effect observations and, consequently, populations' ability to choose what individual adaptations to promote. Lagging a variant a in m time units per time, (2), generates sequential effect observations across m different background conditions, Fig.1(c, middle). Effects of a are now observed after 1, 2, 3, ... time lags, and, thus, in populations under subsequent b, c, d, \dots conditions. These effects are associated with the matrix diagonal. Periodic lags lead therefore to more general effect estimates. Lagging all m variants,† (3), makes the matrix correspond to a Latin-Square ('square'), implemented across time. Any other lags will have environmental changes unequally represented across populations (and be 'unbalanced' in the sense of Experimental Designs). For any variant a , the square's upper triangle contains all populations with a , and the lower, without (the diagonal marking the 'times-of-insertion' for the variant). The sizes of these two time-extended superpopulations are denoted n_a and $n_{\bar{a}}$.

More precisely, a *single* square in systems (2) and (3) enumerate all possible background variations of a stationary environment. These are all variations where the environment does not change its order-of-play. This can be seen by picking any variant in the square and following it horizontally (e.g., $b < c < d < \dots$ for a in Fig.1(c)). As such, they are natural population equilibrium positions. The set of all squares enumerates, in turn, all background variations of non-stationary environments. While this is true for (2-3), under (2) the population can know the effect of only one environmental change, and under (3) of all, simultaneously. The central hypothesis behind the LSM is that the latter is a requirement for selection. Crucially, each previous systems lead to distinct population polymorphism, $\partial n / \partial m^2$, and variant, $\partial n_a / \partial m^2$, mutation rates across environment-population cycles. These asymptotic limits follow directly from the previous lags;‡

*we write a for both a variant and its random indicator of presence, $a \in \{0, 1\}$.

†i.e, with common lag m across all variants and per-variant and time frequency of m .

‡where the population size n required to enumerate all effects in (2-3) grow with m according to an arithmetic series, Fig.1(c, *generated populations*), with common difference (lag) m , and m or m^2 elements in (2-3), leading to

$$(2) \begin{cases} \frac{\partial n}{\partial m^2} = \left(1 - \frac{1}{m}\right)^m \xrightarrow{t} e = 2.71\dots, \\ \frac{\partial n_a}{\partial m^2} = \frac{\partial n}{\partial m^2}, \end{cases} \quad (3) \begin{cases} \frac{\partial n}{\partial m^2} = \frac{1}{2} \left(m - \frac{1}{m}\right)^m \xrightarrow{t} \frac{\phi}{2} = 0.81\dots, \\ \frac{\partial n_a}{\partial m^2} \xrightarrow{t} \frac{1}{2}, \end{cases} \quad (1)$$

where ϕ is the golden ratio. In (3), the per-population and per-variant rates differ. The latter rate follows from the variant's superpopulation relative sizes, $n_a = n_{\bar{a}}$, in the square.

Population structure under external change. The definition of mutation robustness implied by the previous is that of robustness as effect invariance. Effect invariance means that whether we make a change a to a population x_i or another x_j , the observed changes in fitness will be identical in both cases, $y(x_i + a) - y(x_i) = y(x_j + a) - y(x_j) = \Delta y(a)$, for any $x_i, x_j \in X$. Any such measure requires, however, the enumeration of all possible background conditions, x_i , to add a . A m -square's diagonal enumerates all conditions for one variant (stationary), the full square for m variants (stationary), and all m -squares for m variants in non-stationary environments. Systems (2-3) correspond, therefore, to the only systems where effect invariance for one (2), or many (3), mutations can be evaluated and optimized. In them, invariance can be quantified simply by effect observation variance after full background variation[§] $\text{VAR}^{-1}[\Delta y(a \mid \Pi(X - \{a\}))]$. Squares can thus be seen as population structures maximizing invariance, and robustness, under stationary conditions - and an equilibrium position for populations under external changes.

LSM matrices are circulant matrices^{23,25}, which have simple periodic representations, Fig.1(b, right), with frequencies $1/m$ (outer circle) for system (2) and $1/m^2$ (inner circle) for (3). The representation leads to equivalent statistical and algebraic interpretations for mutation robustness. Statistically, a system is effect-invariant if it is able to **sustain small effect variance under full external variation**. This can be indicated by a null Generalized Variance (GV)²³, the determinant of the population's variance-covariance matrix, but only in the previous systems (i.e, with their rates and stationarity assumptions). Algebraically, the square matrix is invariant under changes of basis. The previous definitions lead thus to a coordinate-free definition of effects, as effect observations that remain invariant under all possible changes of basis of the type $x_0 - a$ to $x_0 + a$. The approach has close connections to both the theory of Unbiased Statistics (U-Statistics) and Deep-Learning²³. Both perspectives lead to factorwise linear-systems asymptotically (i.e., towards population effect homogeneity), while allowing for non-linearity outside equilibrium. This is a common pattern in Biological and Economic population-environment systems.

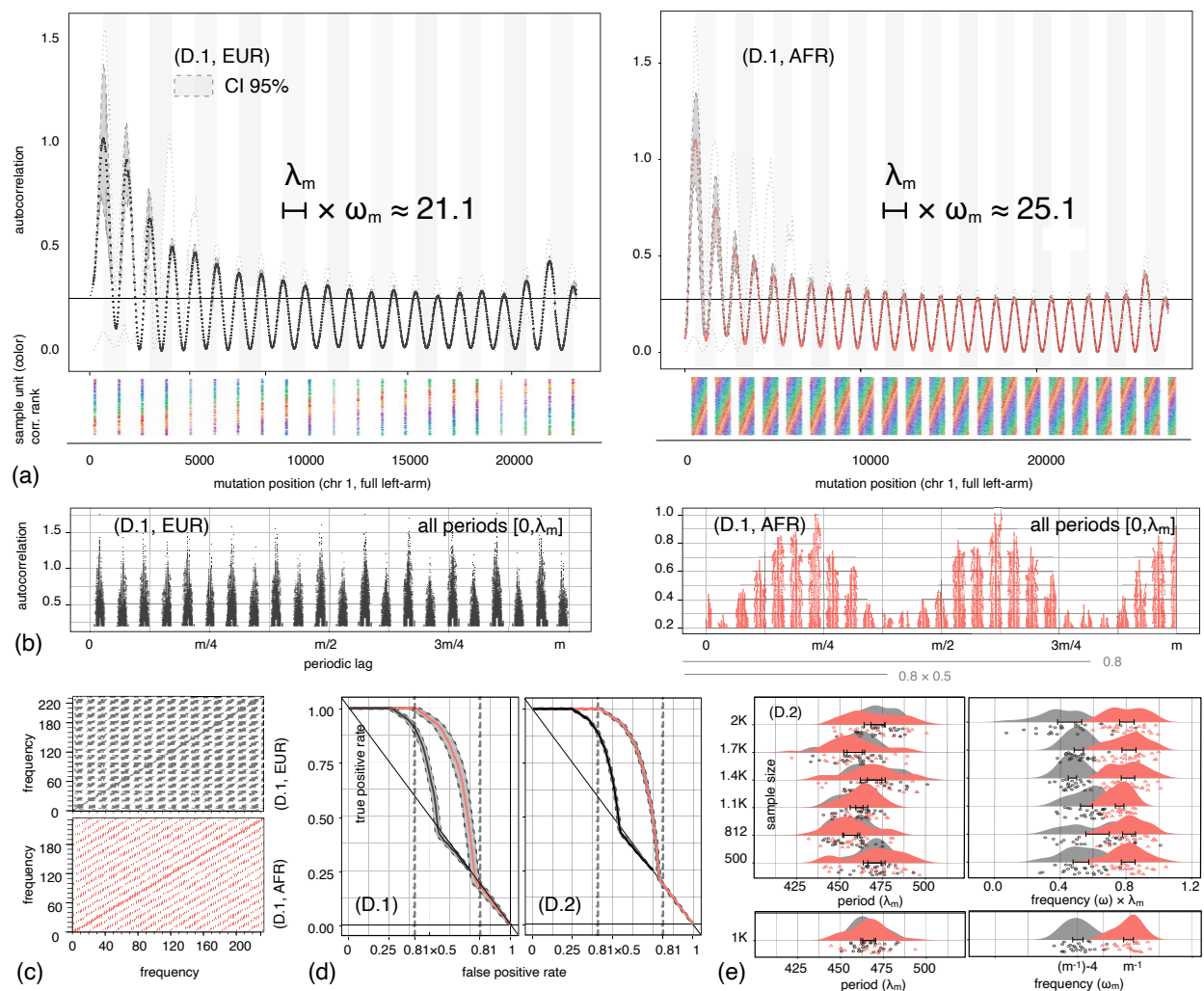


Figure 2 UK Biobank and 1K Genomes (broad time-scale). (a) Autocorrelation $\rho[z(i)]$ over left-arm of human chromosome 1 across European (EUR, $n = 503$, left) and African (AFR, $n = 661$, right) populations of the 1K Genomes project²⁶ (D.1), gray-white bars show LSM predicted number of cycles per genome, ω_m , and their lag period, λ_m , autocorrelation confidence intervals (CIs) are shown as dark gray ribbons, **(lower strips)** population (color) correlation rankings across all sites shows periodic correlation, **(b)** genomic periodicities for EUR and AFR populations according to cumulative autocorrelations $\rho[z(i) - z(i + l)]$ over all integral lags $0 < l \leq \lambda_m$, **(c)** graphical test for periodic correlation, **(d)** SNP survival Empirical ROC curves follow the rates in Eq.(1), **(d)** ω and λ in the UK Biobank²⁷ (D.2)'s UK and African born populations (bootstrap with sample sizes of [500, 2000]), for **(bottom-row)** a single environment-population cycle ω_m , or, **(top-rows)** many ω .

2 Results

Whole-genome Autocorrelation. Fourier and frequency-based representations have been central to many key scientific discoveries (e.g., DNA double-helix and quantum double-slit experiments). Although their relevance to omic data has long been hypothesized^{28,29}, it has led to few empirical results. In fact, the 3-way relation between population diversity, growth and fitness leads fundamentally to periodic functions³⁰. Genome autocorrelation is a (circular) convolution of the full genome with itself, and indicates across-genome patterns of pairwise overlap and differences. The number of differences in populations, s_{ij} , is central to Neutral Theory (NT)³¹. We interpreted them as counts of single effect observations, over distinct differences, a, b, c, \dots , and genetic backgrounds, x_0 . Under NT, for a constant size (diploid) population at equilibrium with S segregating sites, $E[s_{ij}] = E[S/\sum_{i=1}^{n-1} \frac{1}{i}] = 4N\mu$. This celebrated relationship has been re-formulated across theories³², but can also be interpreted in combinatorial grounds, as $\sum_{i=1}^{n-1} \frac{1}{i}$ is the expected number of fixations (overlaps) among random permutations.

We start with the popular 1K genomes dataset²⁶ (D.1). Fig.2(a) shows autocorrelation among all single-nucleotide polymorphism (SNP) positions in the first and largest human chromosome (full left-arm), across all members of the European (EUR, $n = 503$) and African populations (AFR, $n = 661$). The left-to-right y -values indicate correlations at increasing genomic distances. The gray band shows autocorrelation confidence interval (CI) among sites, and the dotted line shows the (min-max) range across all population members. These illustrate the strong regularity in correlations across sites, distances, and members, as would be expected from the common assumption of a homogeneous mutation rate (per evolutionary regime). The solid horizontal line marks the baseline rate of $1/4$, indicating the proportion of sites that remain fixed at a time, as expected by NT.

The first human chromosome has ~ 247 Mbp and genome 6,200 Mbp. According to the previous, genomes of populations in systems of type (3) will have a rate of change of $1/m$ for each of its m positions. We thus expect $\omega_{t=m} \approx 6,200/247 = 25.1$ for chr-1, where ω_m is the per-variant frequency in one population-environment cycle (i.e., in a single square). This simple calculation approximates the frequency (i.e., number of cycles per genome) estimated from all genomes in AFR, Fig.2(a). The EUR population has gone through the out-of-Africa bottleneck^{33,34} and, unlike the AFR, already underwent the second demographic transition. For systems (2-3)²³, $\omega_m^{(2)} = \omega_m^{(3)} - 4$. We thus expect $\omega_m^{(2)} \approx 21.1$ in EUR. Under lower selection pressure, the observed number of cycles decreases according to predicted, while observed lag periods λ remain constant, Fig.2(a). This frequency-period combination suggests the diagonal 'hopping' pattern of (2), Fig.1(c). The pattern can be seen in the populations of low-coverage sequencing datasets (D.1) and, even more clearly, in the subpopulations of high-depth datasets. Fig.2(e, bottom-row) shows number of cycles

$n = (m-1) \times m$, and, $n = (m^2-1) \times m$, Fig.1(c, table), the same limits can be obtained from purely combinatorial and geometrical arguments²³.

[§]where $\Pi(X)$ is the set of all permutations of the elements in X ²⁴.

and periods in the African and British-born populations in the UK Biobank²⁷ (D.2, 1000 bootstraps, 6 different sample sizes in [500, 2000]) for all chromosomes.

Periodic Correlation. Increased frequency ω , with little change in period λ , leads to periodic correlation across the genome. The notion of correlated periodicity is well-studied³⁵. It was depicted in Fig.1(c), and can be demonstrated in different ways. The colored strips in Fig.2(a, bottom) show population members (each a distinct color) ranked by correlation in each genome position. In a square, correlations increase linearly to the right, with variants assuming specific correlation levels periodically, one at a time. The strip depicts these across-genome patterns. Fig.2(c) shows graphical tests for correlation periodicity³⁶ (D.1). In populations that are periodically correlated, observed frequencies in the test are distributed in equally-spaced diagonals. We observe this (in λ segments) for the AFR, but not EUR, population.

According to the previous, systems (2-3) differ in their frequency spectra. System (2) is composed of exponential frequencies (square diagonals), and (3) of exponential (diagonals) and fibonaccian (squares). Fig.2(b) shows cumulative autocorrelations in $z(i) - z(i + l)$, where $z(i)$ are SNP positions²³, and, l are all integral lags $l \in [0, \lambda_m]$. This is a common way of revealing periodicities in time-series. The EUR population has regular frequencies at $1/m$ intervals. The AFR population has a further periodicity: a bisection every $0.81m$ periods. Both are predicted by the LSM. Fig.2(e, top-rows) shows the latter rates across the UK Biobank. They correspond to asymptotic frequencies ω across longer periods, Eq.(1). Distinct rates lead also to distinct autocorrelation patterns across systems, resembling peaks (2) or triangles (3). These results further suggest that systems (2-3), optimal in stationary and non-stationary environments, are associated with populations, respectively, under drift (2) and selection (3). Practitioners will recognize these patterns, alternating present/absent triangles of same base length, from pairwise LD-block plots^{37,38}. The patterns in Fig.2(b) do not correspond to those patterns, but to their generative source. For example, it is consistently observed that LD-blocks extends over distinct distances in AFR and EUR^{39,40}, and that these differences are associated with distinct statistical opportunities (e.g., detect associations in EUR, then perform fine-mapping in AFR^{38,40}).

Mutation Survival and Prediction. Consider two populations with the same founder genome, one under drift and another under selection, evolving during a $[0, t_{max}]$ period. These populations will have distinct combinatorial and statistical landscapes for the selection process. Let $surv_t(x_0 + a)$ be a binary indicator of a SNP a 's survival t generations after its founding mutant. The area-under-the-curve for the time-dependent ROC SNP survival curve indicates

$$Pr [surv_t(x_0 + a) > surv_t(x_0) \mid y(x_0 + a) > y(x_0), t], \quad (2)$$

and selection's ability to rank²³ population fitness after t experimental generations. Fig.3(a-c, left-column) shows empirical ROC curves for variants in *Saccharomyces cerevisiae*⁴⁵ (D.3, artifi-

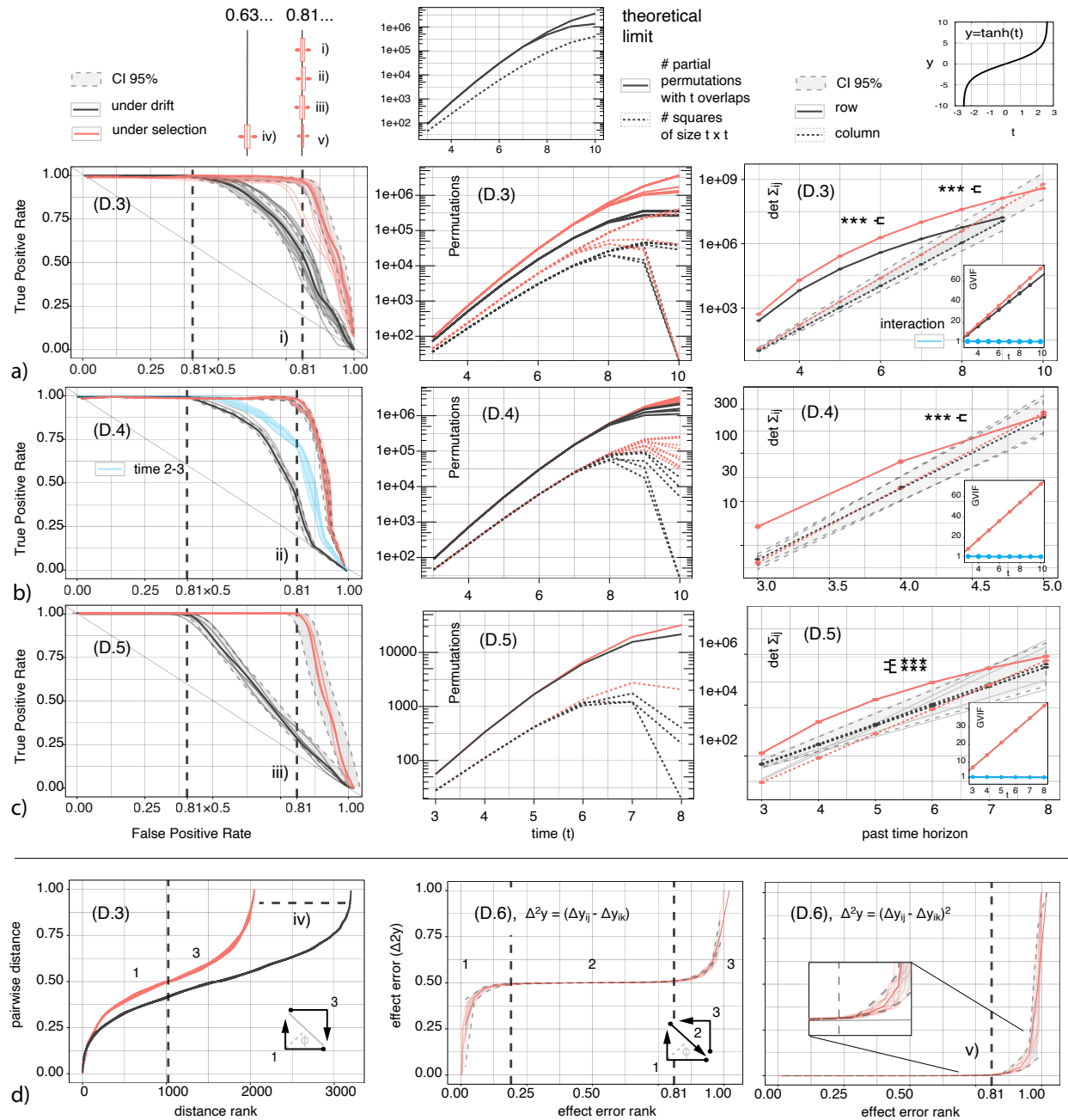


Figure 3 Experimental interventions on selection and effects (fine time-scale).

Experiments over (a) yeast⁴¹ (D.3), (b) fly⁴² (D.4) and (c) E.coli⁴³ (D.5) populations, D.3 and D.5 have populations placed experimentally under selection and D.4 has high selection levels in a single interval, (right) Empirical ROC curves, where dashed lines and box-plot variation (i-iii, top-right panel) show LSM limits, Eq.(1), (middle) theoretical (top panel) and empirical number of (partial) permutations and squares (y-axis in log-scale), (left) Generalized variance ($\det \Sigma_{ij}$) and their inflations (GVIF, lower panels), (d) (left) spatial distances among all pairs of genes in D.3 follow a \tanh function (top-right panel) and e -sized drift-selection increases (boxplot, iv, top-right panel) as expected by the LSM, (middle-right) experimental effect observations in bi-mutation experiments⁴⁴ (D.6) follow LSM functionals and limits.

cial selection, 10 epochs of 100 generations, 2 population replicates), *Drosophila melanogaster*⁴⁶ (D.4, observed high selection in 1 interval, 5 monthly intervals, 10 replicates), and *Escherichia coli*¹ (D.5, artificial selection, 5 generations, 10 replicates) populations. Fig.2(d) shows, in turn, ROC curves with the previous observational datasets, D.1 and D.2, under random sampling.

Under uniform and noiseless selection mechanisms, true positive (TP) rates (y-axis) are associated with fixation rates for mutations that are beneficial across entire populations (and all possible x_0), Eq.(2). Maintenance of 1.0 TP rates across growing populations in D.3-5 are thus indicative of effect invariance²³. With population structure, Fig.2(d), effects are invariant under drift until 1/4 of the full sample, which coincide with their level of pairwise fixations. The increased mutation rates under selection increases the number of background conditions in which effects are observed and, consequently, effect invariance for a larger section of the (combinatorially possible) population. The rate where this transition happens is ~ 0.81 , which is the rate necessary for variants to become simultaneously balanced, Eq.(1). This is seen across all data, D.1-5. By maintaining balance among mutations, increased mutation rates allow effects to remain applicable throughout the diversifying populations, and their full evolutionary trajectories. Understanding how to predict mutation spectra from environment conditions has great practical consequences⁴¹⁻⁴³.

Combinatorial Enumeration. We now take a purely combinatorial perspective on adaptation, in contrast to the statistical of other results. According to the previous, we can characterize populations by the number of effect observations they can generate or enumerate²⁴. A homogeneous population generates none. Systems (2-3) generate the maximum number of backgrounds under which a (limited) set of variant effects are observed. Fig.3(a-c, middle-column) show the number of enumerable permutations across time in D.3-5 (y-axis in log-scale). Curves for populations under drift and selection coincide with two combinatorial limits. On the top-left panel is the theoretical limit of permutations (solid line) with given numbers of fixations (overlaps). Experiment D.3 sustained a selective intervention (stressful, acidic environment) across its 10 time points, while D.4-5 had the intervention concentrated in one point (a natural seasonal change in D.4 and fluorescence-based selection in D.5). In all cases, the Empirical number of permutations had order-of-magnitude increases in the number of permutations (solid) and squares (dotted line) - this difference sustained throughout the entire experiment in D.3. In fact, systems' empirical number of permutations under selection largely follow the theoretical maximum number of both permutations and squares, Fig.3(a-c, middle-column) - a requirement for type (3) systems. This suggests that evolution is constantly pushing populations against (and is limited by) a combinatorial limit on effect observations and their backgrounds. With constant selection (D.3), the number of squares under selection at the end of the experiment coincides with the number of permutations under drift, which indicates that the system has then one square per variant (a limiting condition in parallel adaptation). Experiments with a single intervention, D.4-5, observe a steep increase in the number of squares at the time of intervention ($t = 4$ and $t = 7$) - many replicates going from no squares to the maximum number in this single period.

Generalized Variance. The Generalized Variance (GV) can describe effect invariance in systems (2-3)²³. Fig.3(a-c, right-column) shows sample variance-covariance determinants calculated independently across experiments for populations (row, solid line), $\det \Sigma_{row}$, and time (column, dotted line), $\det \Sigma_{col}$. The figure shows that, as in all complete designs, their row and column-wise GVs coincide⁴⁷, $\det \Sigma_{row} = \det \Sigma_{col}$. It implies, in turn, that across-diagonal variances between environment and populations coincide in $t_{max} \times t_{max}$ matrices (rightmost dots) - a requirement²³ for systems (2-3). The figure also shows what happens as we reduce the time horizon (x-axis) progressively from t_{max} (all generations until the founder) to 3 (generations from t_{max}). This breaks the previous relations, demonstrating how adaptation can be seen as *time-extended* $m \times m$ designs, like the LSM.

The LSM corresponds to a fully-nested model for effect observations, where we rely not only on main effect estimates, but all interaction effects (thus an ANOVA²⁴ with all combinatorial interactions). In this interpretation, all enumerable interactions correspond to all enumerable effect observation backgrounds. Unbiasedness of effect estimation is therefore associated with the unbiasedness of interaction effects in typical designs. Only by keeping balance among background conditions, we can estimate robustness accurately. Periodic population-environment lags of size m fulfill this condition for one or m variants, Eq.(1). As noted by Fox and Monette⁴⁷ (Sect.6), while interaction effects are often ignored in practice, the GV inflation factor (GVIF) is a uniquely suited index to indicate the extent to which population imbalance will compromise interaction effect estimation. In balanced designs, we expect the GVIF of interactions to remain unitary, despite the otherwise large (and, as expected, linear) increases in colinearity. This is also shown in Fig.3(a-c, right-column, lower-panels), with interaction GVIFs shown in blue.

Single Effect Observations. The previous showed the consequences of experimental manipulations on evolutionary regimes (same genome, different regimes). As a representational theory of effects, the LSM can also be evaluated with experiments that, instead, manipulate individual variants (and can thus measure, experimentally, their effects on fitness). Before those results, Fig.3(d, left) shows spatial distances among all pairs of genes in D.3 (normalized, same chromosome and experimental times). According to the LSM, distance ranks in a square follow a tanh function²³, Fig.3(top-right). This is because the number of pairwise distances in a square follow the arithmetic series illustrated in Fig.1(c). Distances among genes are $(1 - 1/e) = 0.63\dots$ times smaller under selection, which corresponds to the $(1 - 1/m)^m$ increase in rate illustrated in Fig.1(b,c) and Eq.(1). The figure also shows this scaling factor's variation (iv, box-plot) across all gene pairs and times.

CRISPR and Temperature-Sensitive (TS) gene editing experiments intervene experimentally on a single gene, adding an allele a , to a genome x_0 , the resulting difference in fitness corresponding to a single effect observation, $\Delta y_{ij} = y(x_0 + a) - y(x_0)$. Costanzo et al.⁴⁴ (D.6) measured such effects for all gene pairs (ij) in yeast. Fig.3(d, middle) shows all pairwise differences among effects (normalized, same chromosomes). The plot (of effect differences) follows the same shape as the one for spatial differences, Fig.3(d, left), with a plateau at 0.5. The plateau corresponds to same, or near, position alleles that are not present in the single and fine experimental time of

Fig.3(d, left). It also illustrates effect invariance, and the condition $(\Delta y_{ij} - \Delta y_{ik})^2 = 0$ across all effect differences from a fixed gene i [¶]. The plateau is also reminiscent of FGM’s frontier, where many effects take antagonistic values randomly.

We can divide the observation of effects for a given variant in 3 phases (before, after and in the frontier). According to the LSM population-wide representation, these correspond to squares’ lower-triangle, diagonal, and upper-triangle, Fig.3(d, lower-right diagrams). Each diagonal represents a ‘cost’ for increased robustness, described by the distinct rates in Eq.(1). This is further illustrated in Fig.3(d, right) which shows *squared* effect differences, and leads to the same 0.8–0.2 limits seen in D.1-5. We can now return to the FGM, whose chief argument was that evolution proceeds by small mutations. The argument has also been its main source of criticism, starting from Kimura⁴⁸, who argued, theoretically, for the importance of intermediate effect sizes to adaptation. Contributions from Gillespie, Orr and Gerrish suggested, now including empirical components, that adaptation is characterized by a combination of exponential and small-sized ‘jumps’ in fitness ranks^{49–51}. The previous not only confirms these findings, but also gives them a specific 0.8–0.2 effect size distribution. Additionally, the previous suggests how effects are spatially distributed across the genome, and how their sizes and spatial distribution change under selection.

3 Conclusion

We formulated the hypothesis that adaptation processes systematically amplify the robustness of their mutations. Robustness is highest under specific patterns of lag and synchronicity between systems and their environments. We demonstrated these patterns in the broad time-scale of high-depth genomic datasets, and the fine-scale of multiple barcoding longitudinal experiments.

The perspective sheds light on fundamental aspects of adaptation, such as its pace and limits. It allowed us to present a complete picture of how sets of whole-genomes change in response to environmental changes, and the essential role of standing variation and population structure in adaptation. The picture is one of adaptation as recursive back-and-forths between environments and populations, where rapidly changing environments prompt, in return, the need for systems to generalize gains across these new conditions. We believe this theoretic-empirical perspective could help transform our understanding of evolution, biodiversity maintenance and medical human genomics.

References

1. Zheng, J., Guo, N. & Wagner, A. Selection enhances protein evolvability by increasing mutational robustness and foldability. *Science* **370**, eabb5962 (2020). URL <https://doi.org/10.1126/science.abb5962>.

[¶]where (jk) are all other same-chromosome genes.

2. Johnson, M. S., Martsul, A., Kryazhimskiy, S. & Desai, M. M. Higher-fitness yeast genotypes are less robust to deleterious mutations. *Science* **366**, 490–493 (2019). URL <https://doi.org/10.1126/science.aay4199>.
3. Chaturvedi, A. *et al.* Extensive standing genetic variation from a small number of founders enables rapid adaptation in daphnia. *Nature Communications* **12**, 4306 (2021). URL <https://doi.org/10.1038/s41467-021-24581-z>.
4. Hernando-Amado, S., Laborda, P., Valverde, J. & Martínez, J. Mutational background influences *p. aeruginosa* ciprofloxacin resistance evolution but preserves collateral sensitivity robustness. *Proceedings of the National Academy of Sciences* **119**, e2109370119 (2022). URL <https://doi.org/10.1073/pnas.2109370119>.
5. Stewart, B. *et al.* The genetic architecture underlying prey-dependent performance in a microbial predator. *Nature Communications* **13**, 319 (2022). URL <https://doi.org/10.1038/s41467-021-27844-x>.
6. Park, Y., Metzger, B. P. H. & Thornton, J. W. Epistatic drift causes gradual decay of predictability in protein evolution. *Science* **376**, 823–830 (2022). URL <https://doi.org/10.1126/science.abn6895>.
7. Scheuerl, T. *et al.* Bacterial adaptation is constrained in complex communities. *Nature Communications* **11**, 754 (2020). URL <https://doi.org/10.1038/s41467-020-14570-z>.
8. Brennan, R. S., Garrett, A. D., Huber, K. E., Hargarten, H. & Pespeni, M. H. Rare genetic variation and balanced polymorphisms are important for survival in global change conditions. *Proceedings of the Royal Society B: Biological Sciences* **286**, 20190943 (2019). URL <https://doi.org/10.1098/rspb.2019.0943>.
9. Draghi, J. A., Parsons, T. L., Wagner, G. P. & Plotkin, J. B. Mutational robustness can facilitate adaptation. *Nature* **463**, 353–355 (2010). URL <https://doi.org/10.1038/nature08694>.
10. Rao, R. & Leibler, S. Evolutionary dynamics, evolutionary forces, and robustness: A nonequilibrium statistical mechanics perspective. *Proceedings of the National Academy of Sciences* **119**, e2112083119 (2022). URL <https://doi.org/10.1073/pnas.2112083119>.
11. LaBar, T. & Adami, C. Evolution of drift robustness in small populations. *Nature Communications* **8**, 1012 (2017). URL <https://doi.org/10.1038/s41467-017-01003-7>.
12. Wilke, C. O., Wang, J. L., Ofria, C., Lenski, R. E. & Adami, C. Evolution of digital organisms at high mutation rates leads to survival of the flattest. *Nature* **412**, 331–333 (2001). URL <https://doi.org/10.1038/35085569>.

13. Krakauer, D. C. & Plotkin, J. B. Redundancy, antiredundancy, and the robustness of genomes. *Proceedings of the National Academy of Sciences* **99**, 1405–1409 (2002). URL <https://doi.org/10.1073/pnas.032668599>.
14. van Nimwegen, E., Crutchfield, J. P. & Huynen, M. Neutral evolution of mutational robustness. *Proceedings of the National Academy of Sciences* **96**, 9716–9720 (1999). URL <https://doi.org/10.1073/pnas.96.17.9716>.
15. Allen, B. *et al.* Evolutionary dynamics on any population structure. *Nature* **544** (2017).
16. Pavlogiannis, A., Tkadlec, J., Chatterjee, K. & Nowak, M. A. Construction of arbitrarily strong amplifiers of natural selection using evolutionary graph theory. *Communications biology* **1**, 71 (2018).
17. Lieberman, E., Hauert, C. & Nowak, M. A. Evolutionary dynamics on graphs. *Nature* **433**, 312 (2005).
18. Félix, M.-A. & Barkoulas, M. Pervasive robustness in biological systems. *Nature Reviews Genetics* **16**, 483–496 (2015). URL <https://doi.org/10.1038/nrg3949>.
19. Fares, M. A. The origins of mutational robustness. *Trends in Genetics* **31**, 373–381 (2015). URL <https://www.sciencedirect.com/science/article/pii/S016895251500089X>.
20. Fisher, S., Ronald Aylmer. *The genetical theory of natural selection* (Clarendon Press, Oxford, 1930). URL <https://www.biodiversitylibrary.org/item/69976>.
21. Tenaillon, O. The utility of fisher’s geometric model in evolutionary genetics. *Annual Review of Ecology, Evolution, and Systematics* **45**, 179–201 (2014). URL <https://doi.org/10.1146/annurev-ecolsys-120213-091846>.
22. Orr, H. A. Theories of adaptation: what they do and don’t say. *Genetica* **123**, 3–13 (2005). URL <https://doi.org/10.1007/s10709-004-2702-3>.
23. Supporting material (2022).
24. Ribeiro, A. F. & Nonato, L. G. The external validity of combinatorial samples and populations. (*Journal of the ACM, Under Review, Supporting Material*) (2021).
25. Pollock, S. D. S. G. Statistical fourier analysis: Clarifications and interpretations. *Journal of Time Series Econometrics* **1** (2009). URL <https://doi.org/10.2202/1941-1928.1004>.
26. Auton, A. *et al.* A global reference for human genetic variation. *Nature* **526**, 68–74 (2015). URL <https://doi.org/10.1038/nature15393>.
27. Halldorsson, B. V. *et al.* The sequences of 150,119 genomes in the uk biobank. *Nature* **607**, 732–740 (2022). URL <https://doi.org/10.1038/s41586-022-04965-x>.

28. Weinberger, E. D. Fourier and Taylor series on fitness landscapes. *Biological Cybernetics* **65**, 321–330 (1991). URL <https://doi.org/10.1007/BF00216965>.
29. Poelwijk, F. J., Krishna, V. & Ranganathan, R. The context-dependence of mutations: A linkage of formalisms. *PLOS Computational Biology* **12**, e1004771– (2016). URL <https://doi.org/10.1371/journal.pcbi.1004771>.
30. Ribeiro, A. F. Competition, diversity and quality. *Physica A* **568**, 125683 (2021).
31. Watterson, G. A. On the number of segregating sites in genetical models without recombination. *Theoretical Population Biology* **7**, 256–276 (1975).
32. McCandlish, D. M. & Stoltzfus, A. Modeling evolution using the probability of fixation: History and implications. *The Quarterly Review of Biology* **89**, 225–252 (2014). URL <https://doi.org/10.1086/677571>.
33. Courtiol, A. *et al.* The demographic transition influences variance in fitness and selection on height and BMI in rural Gambia. *Current Biology* **23**, 884–889 (2013). URL <https://www.sciencedirect.com/science/article/pii/S0960982213004144>.
34. Henn, B. M., Cavalli-Sforza, L. L. & Feldman, M. W. The great human expansion. *Proceedings of the National Academy of Sciences* **109**, 17758 (2012).
35. Ghosh, S. *Asymptotics, Nonparametrics, and Time Series (Chapter 2)* (CRC Press, Boca Raton, FL, 1999). URL <https://www.taylorfrancis.com/books/9781482269772>.
36. Hurd, H. L. & Gerr, N. L. Graphical methods for determining the presence of periodic correlation. *Journal of Time Series Analysis* **12**, 337–350 (1991). URL <https://doi.org/10.1111/j.1467-9892.1991.tb00088.x>.
37. Todesco, M. *et al.* Massive haplotypes underlie ecotypic differentiation in sunflowers. *Nature* **584**, 602–607 (2020). URL <https://doi.org/10.1038/s41586-020-2467-6>.
38. Gabriel, S. B. *et al.* The structure of haplotype blocks in the human genome. *Science* **296**, 2225–2229 (2002). URL <https://doi.org/10.1126/science.1069424>.
39. Frisse, L. *et al.* Gene conversion and different population histories may explain the contrast between polymorphism and linkage disequilibrium levels. *The American Journal of Human Genetics* **69**, 831–843 (2001). URL <https://doi.org/10.1086/323612>.
40. Reich, D. E. *et al.* Linkage disequilibrium in the human genome. *Nature* **411**, 199–204 (2001). URL <https://doi.org/10.1038/35075590>.
41. Wang, X., Zorraquino, V., Kim, M., Tsoukalas, A. & Tagkopoulos, I. Predicting the evolution of *Escherichia coli* by a data-driven approach. *Nature Communications* **9**, 3562 (2018). URL <https://doi.org/10.1038/s41467-018-05807-z>.

42. Nosil, P., Flaxman, S. M., Feder, J. L. & Gompert, Z. Increasing our ability to predict contemporary evolution. *Nature Communications* **11**, 5592 (2020). URL <https://doi.org/10.1038/s41467-020-19437-x>.
43. Nosil, P. *et al.* Natural selection and the predictability of evolution in timema stick insects. *Science* **359**, 765–770 (2018). URL <https://doi.org/10.1126/science.aap9125>.
44. Costanzo, M. *et al.* A global genetic interaction network maps a wiring diagram of cellular function. *Science* **353**, aaf1420 (2016). URL <https://doi.org/10.1126/science.aaf1420>.
45. Nguyen Ba, A. N. *et al.* High-resolution lineage tracking reveals travelling wave of adaptation in laboratory yeast. *Nature* **575**, 494–499 (2019). URL <https://doi.org/10.1038/s41586-019-1749-3>.
46. Rudman, S. M. *et al.* Direct observation of adaptive tracking on ecological time scales in drosophila. *Science* **375**, eabj7484. URL <https://doi.org/10.1126/science.abj7484>.
47. Fox, J. & Monette, G. Generalized collinearity diagnostics. *Journal of the American Statistical Association* **87**, 178–183 (1992). URL <https://www.tandfonline.com/doi/abs/10.1080/01621459.1992.10475190>.
48. Kimura, M. *The Neutral Theory of Molecular Evolution* (Cambridge University Press, Cambridge, 1983). URL <https://www.cambridge.org/core/books/neutral-theory-of-molecular-evolution/0FF60E9F47915B17FFA2620C49400632>.
49. Gerrish, P. The rhythm of microbial adaptation. *Nature* **413**, 299–302 (2001). URL <https://doi.org/10.1038/35095046>.
50. Orr, H. A. The population genetics of adaptation: The adaptation of dna sequences. *Evolution* **56**, 1317–1330 (2002). URL <https://doi.org/10.1111/j.0014-3820.2002.tb01446.x>.
51. Rozen, D. E., de Visser, J. A. G. M. & Gerrish, P. J. Fitness effects of fixed beneficial mutations in microbial populations. *Current Biology* **12**, 1040–1045 (2002). URL <https://www.sciencedirect.com/science/article/pii/S0960982202008965>.